



## Control of the dual mode operation of generator/motor in SOFC/GT-based APU for extended dynamic capabilities

Zhenzhong Jia<sup>a,\*</sup>, Jing Sun<sup>a</sup>, So-Ryeok Oh<sup>a</sup>, Herb Dobbs<sup>b</sup>, Joel King<sup>b</sup>

<sup>a</sup>Department of Naval Architecture and Marine Engineering (NAME), The University of Michigan, Ann Arbor, MI 48109, United States

<sup>b</sup>US Army TARDEC, Non-primary Power Systems Team, Warren, MI 48397-5000, United States

### H I G H L I G H T S

- ▶ SOFC/GT system augmented by battery and dual operating generator/motor (G/M).
- ▶ Pre-conditioning (of G/M load) strategy proposed for load step-up transients.
- ▶ Motoring operation to absorb the excessive power for load step-down transients.
- ▶ Enhanced system performance and loosened battery requirements by dual operating G/M.
- ▶ Better trade-offs between load following and thermal safety management achieved.

### A R T I C L E I N F O

#### Article history:

Received 1 September 2012  
Received in revised form  
25 January 2013  
Accepted 30 January 2013  
Available online 6 February 2013

#### Keywords:

Solid oxide fuel cell (SOFC)  
Gas turbine (GT)  
Auxiliary power unit (APU)  
Load following  
Generator/motor  
Dual mode operation

### A B S T R A C T

The integrated solid oxide fuel cell (SOFC)/gas turbine (GT) system is an appealing power generation solution for mobile applications from energy conversion efficiency point of view. The relatively poor dynamic capabilities of the SOFC/GT system, which are often the results of system characteristics and SOFC operation safety considerations, limit their widespread applications and must be enhanced to meet safe, efficient and fast load following requirements. To this end, the SOFC/GT system can be augmented by an energy storage unit (e.g., battery) and a dual operating generator/motor (G/M). This paper focuses on investigating the G/M dual mode operation and its implications on system transient performance and battery requirements. Active shaft load control is achieved to manage the load transients through: (a) pre-conditioning of the generator power for load step-up transients; (b) absorbing the excessive power by motoring operation for load step-down transients. By taking full advantage of the bi-directional operation of G/M, we show that better trade-offs between power tracking and thermal management can be achieved, power and energy requirements for the energy storage (battery) can be reduced, and overall system performance can be enhanced.

© 2013 Elsevier B.V. All rights reserved.

### 1. Introduction

Integrating high temperature ( $\sim 1000$  K) solid oxide fuel cells (SOFCs) with a gas turbine (GT) is an effective way to develop highly efficient and clean power generation solutions. By leveraging the complementary features of these two power sources, the integrated system could potentially achieve up to 70% fuel-to-electrical efficiency for stationary applications [1–3]. Our previous analysis [4] shows that 35–40% efficiency is attainable for a 5 kW-class hybrid SOFC/GT system designed for mobile applications such as

auxiliary power units (APUs) for military ground vehicles or commercial heavy-duty trucks.

While the concept of SOFC/GT system is very appealing for mobile applications (e.g., APU) from energy conversion efficiency point of view, its feasibility depends critically on the dynamic characteristics of the combined cycle system [5]. In particular, since load following is one of the most essential requirements for mobile applications, the SOFC/GT system must be able to make fast load transients without causing negative impact on the components and system life cycle.

Recent analysis from the literature [7,8] and our own study, however, have revealed that the SOFC/GT system has very limited dynamic capability due to characteristics of the integrated system and stringent operation safety requirements. First, large thermal inertia of the high temperature SOFC and fuel path dynamics often

\* Corresponding author.

E-mail addresses: [zhenzjia@umich.edu](mailto:zhenzjia@umich.edu) (Z. Jia), [jingsun@umich.edu](mailto:jingsun@umich.edu) (J. Sun), [sroh@umich.edu](mailto:sroh@umich.edu) (S.-R. Oh).

**Nomenclature**

$E_{\text{brg}}$	battery energy capacity requirement
$I_{\text{com}}$	SOFC current density command
$J$	shaft's equivalent rotational inertia
$L_{\text{CTCR}}$	limit of cell temperature change rate
$N$	shaft speed
$N_0$	threshold shaft speed
$N_{\text{crt}}$	critical shaft speed
$N_{\text{des}}$	desired pre-transition shaft speed
$N_{\text{min}}$	lower limit of shaft speed
$P_c$	compressor power
$P_{\text{gen}}$	generator power/load
$P_{\text{gen}}^{\text{des}}$	desired generator load

$P_{\text{gen\_SS}}$	steady-state generator power/load
$P_{\text{max}}$	battery power requirement
$P_{\text{net}}$	net power
$P_{\text{net}}^{\text{des}}$	desired net power
$P_{\text{RMS}}$	RMS power tracking error
$P_{\text{SOFC}}$	SOFC electric power
$P_t$	turbine power
$T_{\text{cell}}$	SOFC cell temperature
$t_d$	delay time of fuel supply
$t_r$	ramping time of fuel supply
$t_s$	settling time of transient response
$v_T$	cell temperature change rate
$W_f$	SOFC fuel rate command
$\eta_m$	shaft's mechanical efficiency

lead to slow transient response. Second, while the SOFC is generally able to respond to quick load changes, a sudden large change in SOFC operating condition could seriously impact the components and their life cycle due to thermally induced stresses [7]. Therefore, fast changes in SOFC operation are often prohibited in practice, and the cell temperature is kept fairly constant for high efficiency and long life cycle operation [7,8]. Another phenomenon which has been observed in both real systems and model-based analysis is the temporary large shaft speed drop during transients that might eventually lead to system shut-down [9]. Given the facts that the optimal operating points are located at the boundary of the feasible operation region [9] and the system relies on the close thermal and mechanical couplings of the physical components to achieve high efficiency, it is an extremely challenging task to make fast load transients while maintaining safe and optimal operation. Therefore, effective strategies that can extend the dynamic capabilities of the SOFC/GT system for improved load following performance are becoming critical enablers for the widespread application of SOFC/GT to mobile platforms.

While the design and optimization of the SOFC/GT system have been investigated by the research community for many years, the control and system integration solutions, especially those aimed at addressing dynamic operations, have not been fully explored [5,8]. In Ref. [7], a multi-loop feedback control scheme has been designed by controlling the current, fuel and air flow rates (by manipulating the generator power) for safe part-load transitions. A model-based predictive control (MPC) strategy, which could explicitly handle various operational constraints, has been developed by our group for coordinated power and thermal management of the SOFC/GT system [5]. The essence of these efforts is to find effective operation strategies without modifying the existing system configuration. While these strategies can mitigate the slow transients of the SOFC/GT system, they cannot eliminate the associated power tracking error due to transient response limitations of the SOFC and the long thermal transient due to large thermal inertia of the fuel cell. To improve the system transient performance, alternative solutions that augment the hybrid SOFC/GT system with new features/functionalities, e.g., the variable geometry turbine (VGT) technique [6], have also been investigated.

This study is aimed at developing solutions through control and system integrations to address the fast load following and safe transient operation problems of the SOFC/GT system. In particular, we incorporate energy storage (e.g., battery) to the system to serve as the energy buffer during transients and investigate the generator/motor (G/M) dual mode operation and its implications on system design and operation.

The remainder of this paper is organized as follows: in the next sections the proposed extended hybrid SOFC/GT system

configuration with enhanced dynamic capability is presented. System modeling and operation principles are introduced in Section 2. The G/M dual mode operation and its implications on system transient performance and battery requirements for load step-up and load step-down transients are presented in Sections 3 and 4, respectively, followed by the evaluation of the proposed control strategies and conclusions.

## 2. System description and operation principles

The SOFC/GT system studied in this paper is intended to be used as an auxiliary power unit (APU) for military ground vehicles. The proposed APU (with a rated power around 5 kW) could provide sufficient power to support surveillance and other missions with reduced aural detectability during engine-off operations. The key system components include an SOFC stack, a catalytic burner, a compressor, a turbine, a generator and a heat exchanger.

The combined cycle SOFC/GT system has several energy converting units and relies on the close coupling among these to achieve high system efficiency and reliable operation. As shown in Fig. 1, the air (pre-heated by the heat exchanger) is supplied to the cathode side of the SOFC, while pre-reformed fuel is fed to the anode side. The combined cathode and anode exhaust from the fuel cell stack can then be fed into a catalytic burner where the unused fuel is burned to increase the temperature of the flow, which will be used to drive the turbine. This provides a mechanism to recuperate the exhaust energy for improved system efficiency. The turbine drives both the compressor (delivers air to the fuel cell stack) and the generator (produces additional electric power during normal operation) through a mechanical shaft.

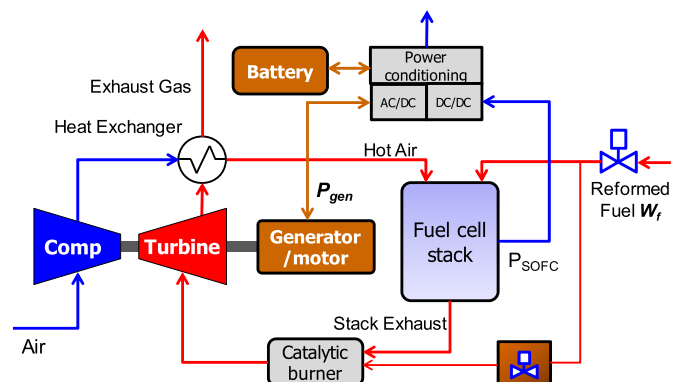


Fig. 1. Schematic of the proposed SOFC/GT hybrid power system.

The high temperature exhaust from the turbine can be fed into the heat exchanger to pre-heat the compressed air delivered to the SOFC.

The strong thermal and mechanical coupling in the hybrid SOFC/GT system, while essential for high system efficiency, complicates the system operation. At the same time, the lack of independent air control severely limits dynamic capabilities and the load following performance of the SOFC/GT system. To ease the power tracking operation and enhance transient capabilities, the SOFC/GT system is augmented with new components and functionalities, as shown in Fig. 1. First, an energy storage unit (a battery or capacitor pack) is included to serve as the energy buffer during load transients. Second, the electric rotational machine will be used as either a generator during normal operation or a motor (driven by the battery or the SOFC electrical output) when there is not enough turbine power for air delivery. This G/M dual mode operation, which is similar to the electrically assisted turbocharger [10] used to improve the performance of automotive engines, has not been found in SOFC/GT systems in the literature, to the best of our knowledge. Meanwhile, the motoring mode operation can also be used to (entirely or partially) absorb the excessive power during load step-down transients, thereby reducing the battery requirements. Third, the burner has its own fuel delivery system to allow the turbine/generator to take on greater load during transients, thereby allowing the SOFC to operate at a relatively constant load condition, thus mitigating the slow dynamic response. The goal of this study is to explore the performance enhancement brought by the newly introduced components/functionalities through model-based analysis. In particular, we seek control solutions that can take advantage of the G/M dual mode operation, and quantify the benefits in terms of power tracking performance and energy storage (battery) requirements.

First principle based tubular SOFC model developed in Ref. [11] is used in this study. The SOFC model, which is developed by considering the electrochemical reactions, mass and energy balances, uses a finite volume method for discretization [8,9]. For the turbomachinery, the speed flow characteristics are captured by the compressor and turbine maps [9]. The shaft rotational dynamics is determined by the turbine power  $P_t$ , the power required to drive the compressor  $P_c$ , and the power produced by the generator  $P_{gen}$  as:

$$\frac{dN}{dt} = \frac{P_t \cdot \eta_m - P_c - P_{gen}}{(2\pi/60)^2 \cdot N \cdot J} \quad (1)$$

where  $N$  is the shaft speed in rpm,  $\eta_m$  is the shaft's mechanical efficiency, and  $J$  is the equivalent rotational inertia (sum of the rotor, compressor and turbine inertia) about the shaft axis [9]. The catalytic burner [9] and the (counter-flow) heat exchanger [13] have also been modeled. Interested readers can refer to Refs. [9,11,12] for detailed modeling assumptions and results. It should be noted that the fuel reformer, which has poor dynamic capability, is not explicitly included in this paper. However, its poor dynamic capability and the implications on SOFC/GT system operation are considered, as explained in Section 3.1 and Fig. 3.

Without the battery, the system has three control inputs, namely, the fuel rate ( $W_f$ ), the SOFC current density ( $I_{com}$ ), and the generator power ( $P_{gen}$ ). Fig. 2 shows the steady-state feed-forward map of the optimal set-points (i.e., achieving the highest fuel efficiency) of these inputs with respect to the net power demand ( $P_{net}$ ). Note that the total power output of the system is the sum of  $P_{SOFC}$  (output power of the SOFC) and  $P_{gen}$ . In addition, the overall efficiency of the system is around 45% (improvement over the results of Ref. [4] due to the addition of the heat exchanger), over a wide load range.

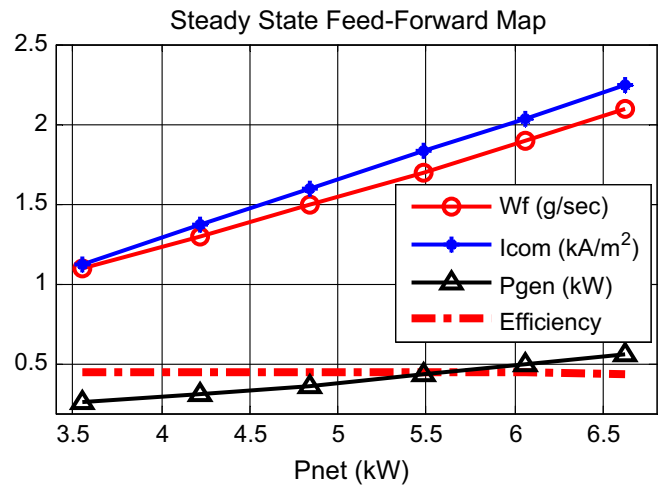


Fig. 2. Steady-state optimal set-points for current density ( $I_{com}$ ), fuel rate ( $W_f$ ) and generator power ( $P_{gen}$ ) as a function of the net power demand ( $P_{net}$ ).

The focus of this paper is to investigate the G/M dual mode operation and its implications on energy storage sizing and system operation. In particular, we will study whether the motoring operation can help in (a) eliminating system shut-down (usually caused by large shaft speed drop during load step-up transients); (b) improving the transient responses; and (c) reducing the battery power and energy requirements. Since the G/M transient is much faster than those of the SOFC and GT, we assume that instantaneous control of the G/M load can be achieved in our investigation. We first investigate the control authority of G/M and the feasibility of using the G/M for transient control through a case study.

### 3. Case study of G/M for load step-up

In this section, the G/M dual mode operation will be investigated through the load step-up transition from 4.2 kW to 6.06 kW (at time  $t_1$  in Fig. 3), which correspond to the optimal set-points A and B in Table 1, respectively.

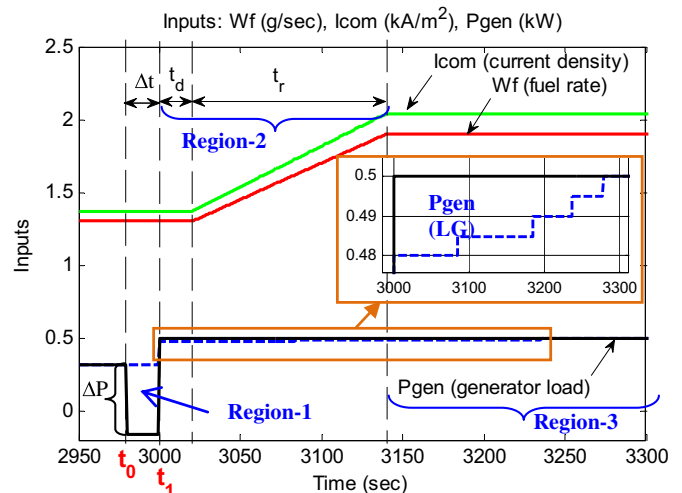


Fig. 3. Illustration of the load power demand step-up transition operation from 4.2 kW to 6.06 kW at time  $t_1$ . The G/M dual mode operation is evaluated by combining the pre-conditioning (applied at region-1: [ $t_0, t_1$ ]) of the generator load with the load governor (LG, applied after time  $t_1$ ). Region-2 deals with fuel path delay and dynamics, while the system settles down at the end of region-3.

**Table 1**  
Feed-forward optimal set-points used for case studies in this paper.

Inputs	$W_f$ (g s <sup>-1</sup> )	$I_{com}$ (A m <sup>-2</sup> )	$P_{gen}$ (kW)	$P_{net}$ (kW)
Set-point A	1.3	1370	0.32	4.20
Set-point B	1.9	2040	0.50	6.06
Set-point C	1.5	1580	0.34	4.77

3.1. Analysis of the load step-up operation

Considering Fig. 3, ideally, the inputs to the SOFC/GT system can be stepped up instantaneously at time  $t_1$  for fast load transition. However, it has been shown that such operation can cause system shut-down due to sudden shaft speed drop [9]. Instead, the fuel rate ( $W_f$ ) and the current density ( $I_{com}$ ) commands to the SOFC should be changed slowly for safe transient operation. Besides the fuel path dynamics (which can be represented by the fuel supply ramping time  $t_r$ ), there is also some delay ( $t_d$ ) caused by the fuel supply/reforming system, as illustrated in Fig. 3. To avoid possible hydrogen starvation and burner over-heating [9], the current density command should be adjusted accordingly to match the fuel supply (i.e.,  $t_i(I_{com}) = t_i(W_f)$ ,  $i = d, r$ ). This simplified approach (i.e., use of fuel supply ramping time  $t_r$  and delay time  $t_d$ ) is expected to be a reasonable representation of the effect of the complex fuel reforming (has slow dynamics) and supply system, given the focus of this paper is to investigate the G/M dual mode operation.

With  $W_f$  and  $I_{com}$  as given in Fig. 3, our simulation shows that the system could experience a shut-down if the generator load  $P_{gen}$  is stepped up from 0.32 kW to 0.50 kW (the optimal values according to Table 1) at time  $t_1$ . This is because the increase in  $P_{gen}$  deprives the turbocharger from having enough power for air supply during the transient to support the SOFC operation, causing the turbo-shaft to stall, as shown in Fig. 4. To achieve fast load following while avoiding shut-down, one can identify the maximum permissible step change of  $P_{gen}$  at each time step [9] by solving the following optimization problem:

$$\min_{P_{gen}} (P_{gen}^{des} - P_{gen}) \tag{2}$$

$$\text{subject to : no system shut - down and } P_{gen}^{des} \geq P_{gen} \tag{3}$$

where  $P_{gen}^{des}$  is the desired generator load.

The solution to Eq. (2) can be reformulated as the load governor (LG) problem as:

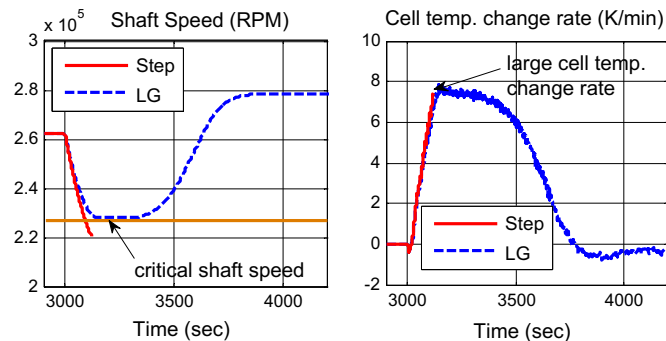


**Fig. 4.** Load step-up transient responses ( $t_d = 20$  s,  $t_r = 120$  s). A direct step-up command from  $P_{gen}(A)$  to  $P_{gen}(B)$  at  $t_1$  causes the shaft speed to drop below the critical shaft speed, which eventually leads to system shut-down. A load governor (LG) can be used to manipulate  $P_{gen}$  for shut-down mitigation.

$$P_{gen}(k + 1) = P_{gen}(k) + \lambda (P_{gen}^{des}(k) - P_{gen}(k)) \tag{4}$$

$$\max \lambda, \quad \lambda \in [0, 1], \quad t \in [t_1, T] \text{ subject to (3)}$$

where  $\lambda$  is calculated for each time step by a one-dimensional (1-D) optimization search, and  $T$  is the end of the simulation horizon. The LG result is shown in Fig. 3 (for the input) and Fig. 4 (for the shaft speed). Note that for this moderate step-up power transition, since  $P_{gen} > 0$  for all the time, motoring mode operation ( $P_{gen} < 0$ ) is not required for shut-down mitigation. However, the LG results of Figs. 3 and 4 also reveals two issues: (a) the large speed drop at the onset of power step-up, making the shaft speed close to the critical shaft speed ( $N_{crit}$ ), which corresponds to the lower boundary of the feasible operating region of the compressor; and (b) the relatively large cell temperature change rate. Safer load transients can be achieved if we impose a more stringent limit  $N_{min}$  ( $N_{min} \geq N_{crit}$ ) of shaft speed in the LG design.

3.2. Leveraging G/M dual mode operation: a feasibility study

Given that the rapid shaft speed drop (caused by the increase of  $P_{gen}$ ) was shown to be the main cause of system shut-down, an intuitive solution is to increase the shaft speed by reducing  $P_{gen}$  or running the generator in motoring mode ( $P_{gen} < 0$ ) to safely guide the system through the transient. This operation is referred to as “pre-conditioning” of  $P_{gen}$  (region-1 in Fig. 3) throughout this paper. In particular, we would like to investigate the implication of pre-conditioning on transient performance and energy storage requirements. To this end, six different cases (Table 2), with different levels of G/M load for pre-conditioning, are implemented together with the LG to understand the effects of the strategy.

For the case study, the same fuel rate and current density profiles ( $t_d = 20$  s,  $t_r = 120$  s, refer to Fig. 3 for the plots) are used, while different generator loads are applied in the pre-conditioning ( $\Delta t = 20$  s) phase. Six different scenarios are considered in Table 2, including the baseline case (#1, LG without pre-conditioning), one with reduced generator load (#2), one removing the generator load (#3), and three with different motoring operations (#4, 5, 6). The LG is used to identify the  $P_{gen}$  profile after pre-conditioning. The results are shown in Fig. 5 and Table 3.

From Fig. 5, we see that better power tracking performance and smaller cell temperature rates of change are achieved by pre-conditioning of  $P_{gen}$ . Meanwhile, compared with the baseline case, the minimum shaft speed is kept relatively far away from the critical shaft speed for the last three cases. This is mainly due to the fast shaft speed increase enabled by motoring operation during the pre-conditioning phase, as shown in Fig. 5(b).

The performance of different power transients is further analyzed in Table 3 in three different aspects, namely: (a) the power response and load following performance measured by the settling time  $t_s(P)$  and the RMS power tracking error  $P_{RMS}$ ; (b) the battery sizing requirements indicated by the battery’s maximum discharging power  $P_{max}$  and the energy capacity  $E_{brg}$ ; and (c) thermal stress measured by the maximum cell temperature change rate  $\max(v_T)$  and the temperature settling time  $t_s(T_{cell})$ .

**Table 2**  
Generator load during the pre-conditioning phase.

Case	$P_{gen}$ (W)	$\Delta P$ (W)	Note
#1	320	0	Baseline: LG
#2	160	-160	Reduced $P_{gen}$ for pre-conditioning + LG
#3	0	-320	Disengaging the generator for pre-conditioning + LG
#4	-160	-480	Motoring mode + LG
#5	-320	-640	Motoring mode + LG
#6	-480	-800	Motoring mode + LG

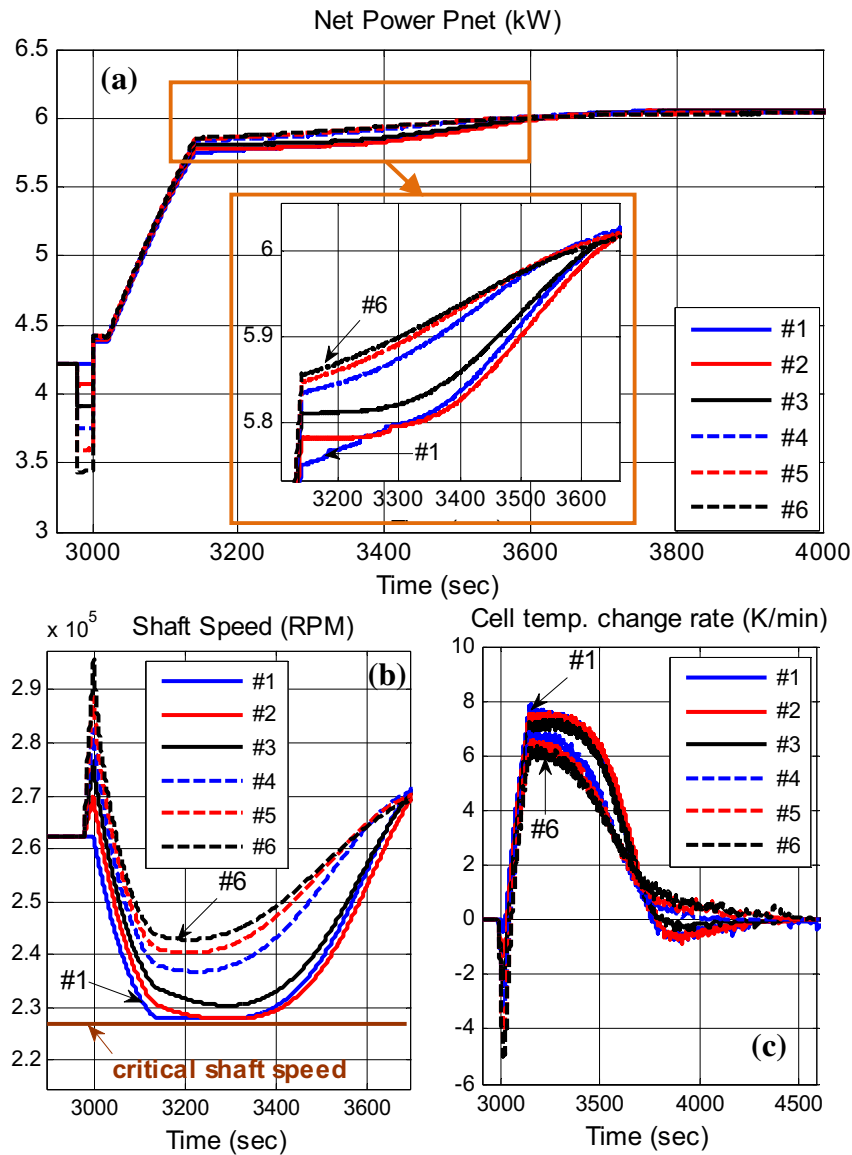


**Fig. 5.** System performance for the load step-up ( $t_d = 20$  s,  $t_r = 120$  s,  $\Delta t = 20$  s) transient: (a) net power response; (b) the shaft speed; and (c) the cell temperature change rate. By reducing  $P_{gen}$  in the pre-conditioning phase from case #1 to case #6, the minimum shaft speed keeps increasing while the maximum cell temperature change rate keeps decreasing.

As shown in Table 3, the proposed pre-conditioning of  $P_{gen}$  provides improvements to the system performance for most attributes, some more pronounced than others:

- It shortened power settling time (up to 15%) and reduced power tracking error (up to 6%);
- It lessened energy storage requirements (up to 15% smaller bridging energy capacity requirement); and

- It reduced (up to 20%) the maximum cell temperature change rate (i.e., safer thermal transient).

In addition, further reduction in the generator load  $P_{gen}$  (i.e., increasing the motoring power) offered very limited or no further improvement of the overall performance as shown in case #5 and case #6, when compared with case #4. This is especially true for the power tracking performance and the energy storage requirements.

**Table 3**

Results of load step-up transients ( $t_d = 20$  s,  $t_r = 120$  s,  $\Delta t = 20$  s).

Case	#1	#2	#3	#4	#5	#6
$T_s(P)$ [s]	560 (100%)	576 (102.9%)	552 (98.6%)	488 (87.1%)	476 (85.0%)	476 (85.0%)
$P_{RMS}$ [W]	585.73 (100%)	601.77 (102.7%)	564.90 (96.4%)	551.26 (94.1%)	552.68 (94.4%)	556.90 (95.1%)
$P_{max}$ [W]	1681.29 (100%)	1655.14 (99.0%)	1647.93 (98.0%)	1636.47 (97.3%)	1633.79 (97.2%)	1631.38 (97.1%)
$E_{brg}$ [kJ]	245.67 (100%)	242.00 (98.5%)	233.25 (94.9%)	210.32 (85.6%)	207.61 (84.5%)	207.95 (84.7%)
$\max(v_T)$ [ $K \min^{-1}$ ]	7.70 (100%)	7.60 (97.4%)	7.20 (93.5%)	6.70 (87.0%)	6.37 (82.7%)	6.10 (79.2%)
$T_s(T_{cell})$ [s]	900 (100%)	940 (104.4%)	620 (68.9%)	710 (78.9%)	830 (92.2%)	1000 (111.1%)

### 3.3. Pre-conditioning strategy for load step-up transients

The case study provides evidence that the G/M dual mode operation has the benefit of improving operating safety and load following performance. In particular, we see that system shut-down can be avoided by pumping additional mechanical energy into the shaft through motoring operation. In order to achieve fast (i.e., minimum RMS power tracking error  $P_{RMS}$ ) and safe (i.e., with limited cell temperature change and away from the critical shaft speed  $N_{crit}$ ) load following performance, we formulate the following trajectory planning problem:

$$\begin{aligned} & \min_{P_{gen}} \sum (P_{net} - P_{net}^{des})^2 \\ & \text{subject to} \\ & (1) \text{ no system shut - down} \\ & (2) \text{ shaft speed} \geq N_{min} (N_{min} \geq N_{crit}) \\ & (3) |dT_{cell}/dt| \leq L_{CTCR} \text{ (safe thermal transient)} \end{aligned} \quad (5)$$

where  $L_{CTCR}$  is the limit of cell temperature change rate.

However, the trajectory planning problem formulated in Eq. (5) is difficult to solve due to its large dimension and complex system dynamics, thereby making online implementation impossible. Therefore, we propose an alternative solution as follows: First, through an off-line process, we determine the minimum shaft speed increase that is required to sustain the system operation before the load increase is applied. This is equivalent to determining the required additional energy that should be pumped into the shaft by motoring operation (or reducing  $P_{gen}$ ) in the pre-conditioning phase. Once this speed is determined, the pre-conditioning strategy is formulated by solving a 1-D optimization problem. Second, once the desired shaft speed  $N_{des}$  is achieved by pre-conditioning, the controller is switched to the LG to increase  $P_{gen}$  to achieve fast load following.

Using the SOFC/GT system model,  $N_{des}$  is determined, for different power transition scenarios, by a 1-D bisectional search algorithm. Given an initial ( $P_1$ ) and final ( $P_2$ ) power level, the incremental shaft speed  $\Delta N(P_1 \rightarrow P_2)$  is the required shaft speed increase to make a safe transition, and this becomes the goal of the control in the pre-conditioning phase. The results of the bisectional search are shown in Fig. 6, where  $\Delta N = 0$  implies that pre-conditioning is not necessary. When  $\Delta N > 0$ , pre-conditioning control will be activated to determine the optimal G/M load to achieve  $N_{des}$ . The results of Fig. 6 are stored as a look-up table (LUT) for online implementation.

To achieve the desired pre-transition shaft speed  $N_{des}$ , the G/M load  $P_{gen}$  during the pre-conditioning phase can be determined in

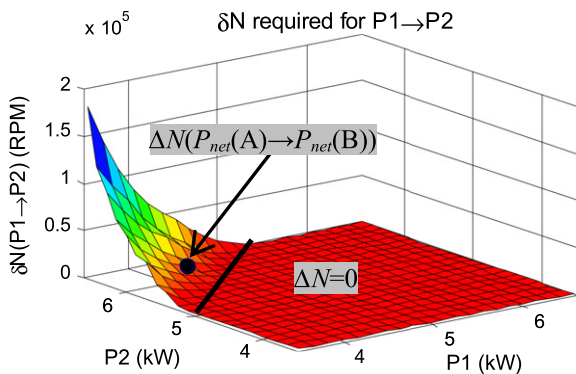


Fig. 6. The look-up table (LUT) for  $\Delta N(P_1 \rightarrow P_2)$ . The solid line is the upper boundary for the region of  $\Delta N = 0$ , i.e., no pre-conditioning of  $P_{gen}$  is required for a safe step-up transition in the lower-right direction of this curve.

the following manner. At each sampling time  $t \in [t_0, t_1)$  (i.e., the pre-conditioning phase), consider:

$$P_{gen}(\tau) = P'_{gen} \quad \text{for } \tau \in [t, t_1) \quad (6)$$

where  $P'_{gen}$  is determined by solving:

$$\begin{aligned} & \max P'_{gen} \\ & \text{subject to } N(t_1) \geq N_{des} \end{aligned} \quad (7)$$

where  $N_{des} = N(P_1) + \Delta N$  with  $N(P_1)$  being the steady-state shaft speed corresponding to the power level  $P_1$  and  $\Delta N$  given by Fig. 6. Note that since  $dN/dP_{gen} < 0$ , the optimization problem (7) is well-posed and has a unique solution. The solution to Eq. (7) can be found by using 1-D optimization search such as bisectional algorithm starting from the search region  $[P_{fsb}, P_{infsb}]$  for each time  $t$  in  $[t_0, t_1)$ , where  $P_{fsb}$  and  $P_{infsb}$  are a feasible and an infeasible input respectively for the pre-conditioning operation. In order to reduce the computational cost of online implementation, the following procedure (Fig. 7) can be used to reduce the size of the initial search region.

As shown in Fig. 6, the desired shaft speed increase for a load step-up transition from  $P_{net}(A)$  to  $P_{net}(B)$  with  $W_f$  and  $I_{com}$  given in the previous case study ( $N_{min} = N_{crit}$ ) is  $\Delta N = 12,853$  rpm. With  $P_{fsb} = -320$  W and  $P_{infsb} = 320$  W, the desired G/M load for the pre-conditioning phase, which is determined by using the algorithm given in Fig. 7, is  $P_{gen}(t) = 30$  W for  $t \in [t_0, t_1)$ . When there is a disturbance in the system,  $P_{gen}(t)$  determined by the algorithm will vary with time, as the state, which may be different from the predicted value, will be fed back at each time instant in the 1-D optimization procedure.

### 4. Case study of G/M for load step-down

In this section, we investigate the G/M dual mode operation for downward load transition through an example of step change from 6.06 kW to 4.77 kW (at time  $t_0$  in Fig. 8), which correspond to the optimal set-points B and C in Table 1, respectively.

#### 4.1. Analysis of load step-down operation

Transient issues associated with downward load transition are quite different from those in upward transition. While system shut-down is not an issue in this case, the slow transient and large power tracking error are the main concerns. As discussed in previous sections, slowly ramping commands for the fuel rate  $W_f$  and the

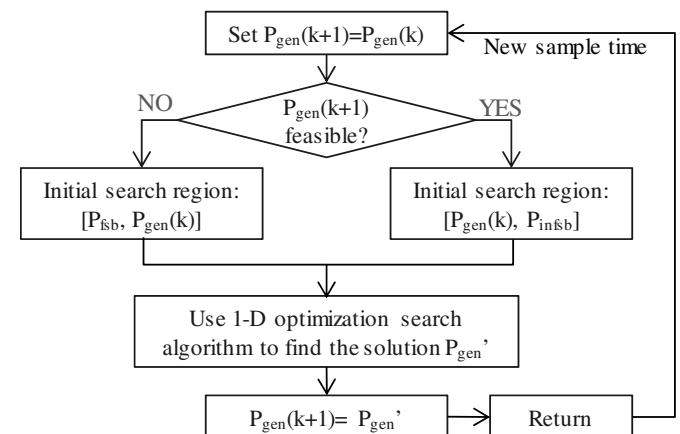


Fig. 7. Flowchart to identify the G/M load for the pre-conditioning phase.

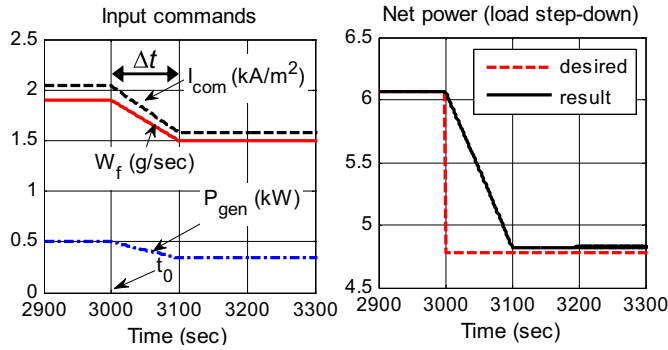


Fig. 8. The inputs ( $\Delta t = 100$  s) and the net power response for the baseline case (also case #1 in Table 4) during load step-down operation.

current density  $I_{com}$  should be applied to the SOFC for safe operation. If  $P_{gen}$  is adjusted (ramped down) accordingly (baseline: case #1 in Table 4), there will be a considerable power tracking error caused by power over-production, as shown in Fig. 8. Intuitively, the excessive (i.e., over-produced) power can be absorbed by the battery for fast load following. It can also be (entirely or partially) absorbed by operating the generator at motoring mode ( $P_{gen} < 0$ ), thereby reducing the battery power and energy requirements. The G/M dual mode operation and its implications on load step-down transient operation and the battery requirements will be investigated in the sequel.

4.2. Fast load following by G/M dual mode operation

Analogous to Eq. (5) for load step-up transitions, a trajectory planning problem can be formulated for fast load following (i.e., minimize  $P_{RMS}$ ) for load step-down transitions as:

$$\begin{aligned} \min_{P_{gen}} \quad & \sum (P_{net} - P_{net}^{des})^2 \\ \text{subject to} \quad & |dT_{cell}/dt| \leq L_{CTCR}(\text{safe thermal transient}). \end{aligned} \tag{8}$$

Similar to Eq. (5), the trajectory planning problem formulated in Eq. (8) is difficult to solve due to of its large dimension. Therefore, alternative solutions should be developed. Because of the large thermal inertia, the SOFC's electric power  $P_{SOFC}$  is dominated by the  $W_f$  and  $I_{com}$  commands during the transient. Therefore, we can predict  $P_{SOFC}$  by using the SOFC/GT model and pre-schedule the G/M load to compensate for the slow transient of  $P_{SOFC}$ . The pre-scheduled  $P_{gen}$  control (#2 in Table 4), which is specifically designed for this particular case ( $W_f$  and  $I_{com}$  given in Fig. 8), can be expressed as:

$$P_{gen}(t) = \begin{cases} -800 + 10.4(t - t_0) & (t_0 \leq t < t_0 + 100) \\ 240 + 0.5(t - t_0 - 100) & (t_0 + 100 \leq t < t_0 + 300) \\ 340 = P_{gen,SS}(C) & (t \geq t_0 + 300). \end{cases} \tag{9}$$

Table 4  
G/M dual mode operation during load step-down transients.

Case #	Control of the generator load $P_{gen}$
1	Baseline case: direct ramp down from $P_{gen}(B)$ to $P_{gen}(C)$
2	Pre-scheduled $P_{gen}$ control for fast load following
3	Direct $P_{gen}$ compensator for fast power tracking
4 and 5	Feedback control for coordinated power and thermal management

An alternative way is to use  $P_{gen}$  to directly compensate the SOFC power  $P_{SOFC}$ , which can be simply calculated by measuring the cell voltage and current. Therefore, a direct  $P_{gen}$  compensator by using:

$$P_{gen} = P_{net}^{des} - P_{SOFC} \tag{10}$$

has also been investigated for fast load following in case #3.

As shown in Fig. 9(a) and (b), both the pre-scheduled  $P_{gen}$  control (#2) and the direct  $P_{gen}$  compensator (#3) achieved extremely good power tracking performance through G/M dual mode operation. However, the excellent load following performance is achieved by risking thermal transient safety (the cell temperature should be changed slowly for safe operation of the fuel cell), e.g., the Siemens–Westinghouse tubular SOFC often requires a 4–6 h start-up time [1], which corresponds to a temperature gradient of  $\sim 4$  K  $\text{min}^{-1}$ . This requirement can be smoothed by using a micro-tubular SOFC [14,15], which has a high thermal shock resistance). As shown in Fig. 9(c) and (d), rapid cell temperature

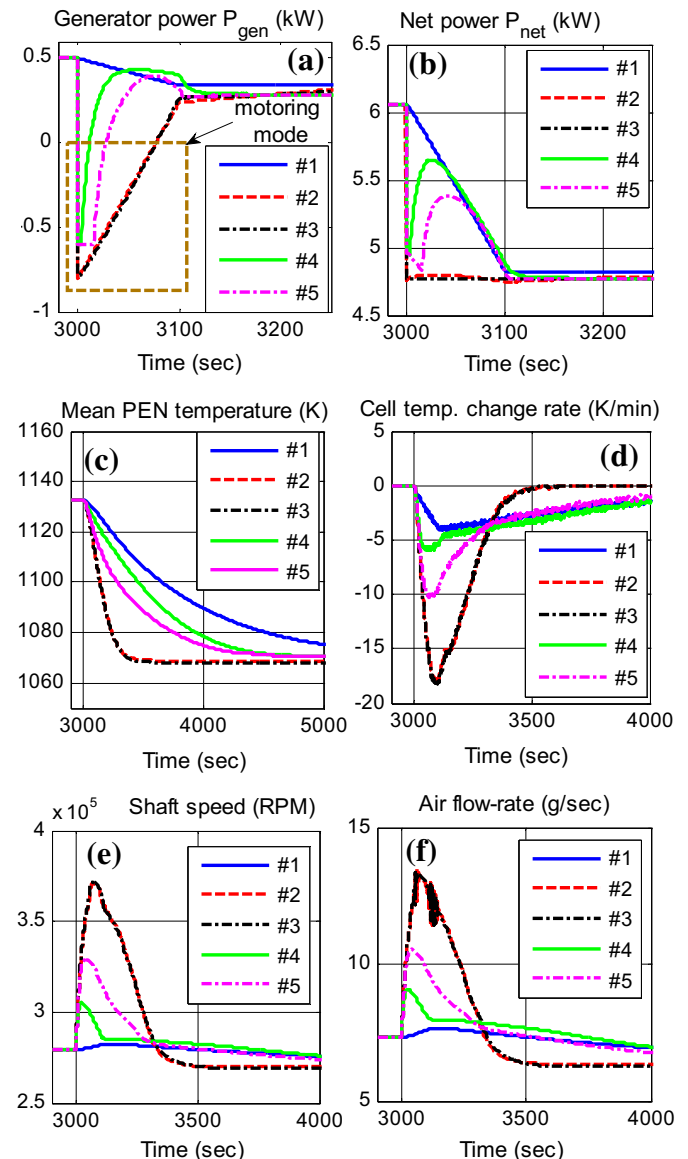


Fig. 9. Transient response during load step-down transients ( $\Delta t = 100$  s).

**Table 5**  
Results of load step-down transients.

Case	#1	#2	#3	#4	#5
Ts(P) [s]	~100 (100%)	~0 (~0.0%)	0 (0.0%)	~100 (100%)	~100 (100%)
$P_{RMS}$ [W]	773.6 (100%)	17.2 (2.2%)	0.0 (0.0%)	622.9 (80.5%)	432.4 (55.9%)
$P_{max}$ [W]	1288 (100%)	25.3 (2.0%)	0.0 (0.0%)	878.0 (68.2%)	610.0 (47.4%)
$E_{brg}$ [kJ]	68.6 (100%)	1.1 (1.6%)	0.0 (0.0%)	57.6 (84.0%)	39.0 (56.9%)
$\max(v_T)$ [K min <sup>-1</sup> ]	4.0 (100%)	<b>18.1</b> (453%)	<b>18.1</b> (453%)	5.8 (145%)	10.0 (250%)
Ts( $T_{cell}$ ) [s]	2468 (100%)	350 (14.2%)	350 (14.2%)	1450 (58.8%)	1153 (46.7%)

Bold value signifies the cases in which the excessive (e.g., >10 °C/min) cell temperature changing rate, which might damage the SOFC permanently.

(which is represented by the temperature of the positive electrolyte negative (PEN) structure of the SOFC in Fig. 9(c)) drop and large cell temperature change rate can be observed for cases #2 and #3. The reason is that the motoring operation (or fast reduction of  $P_{gen}$ ) accelerates the shaft rapidly, as shown in Fig. 9(e). Consequently, more air is delivered to cool the SOFC very quickly, as shown in Fig. 9(f) and (c). Therefore, it can be concluded that fast load following and safe thermal transients are two competing objectives, due to the strong correlation between the cell temperature change rate, the air flow rate, and the shaft speed.

4.3. Balancing power tracking and thermal management

To balance fast load following and safe thermal transient, which are competing against each other, a feedback control scheme, which can be expressed as:

$$P_{gen} = \{P_{net}^{des} - P_{SOFC}\} + \{k \cdot (N - N_0) \cdot 1(N \geq N_0)\} \quad (11)$$

is proposed for the coordinated power and thermal management in case #4 and #5. The first term of Eq. (11), which is identical to the

direct  $P_{gen}$  compensator Eq. (10), is used for power tracking. A proportional controller, the second term of Eq. (11), is designed to limit the shaft speed, thereby limiting the cell temperature change rate to a reasonable range, as shown in Fig. 9(d). The proposed thermal management is developed based on the strong correlation between the shaft speed and the cell temperature change rate, as shown in Fig. 9. The proposed shaft speed controller (10) has two design parameters: the proportional gain  $k$  and the threshold  $N_0$ , the latter of which is used to activate the thermal management function.

Detailed results for the load step-down transition are given in Table 5. Almost instantaneous load following can be achieved by the pre-scheduled  $P_{gen}$  control (#2) and the direct  $P_{gen}$  compensator (#3). However, they induce unacceptably large cell temperature change rate. The proposed coordinated power and thermal management, has moderate load following performance (#4 and #5), as expected. Moreover, the cell temperature change rates are limited to a relatively reasonable range for safe SOFC operation. Therefore, the proposed coordinated power and thermal control (10) can manage the trade-offs between cell temperature and power transients effectively. In addition, compared with the baseline case (#1), reduced battery requirements, i.e., reduced battery

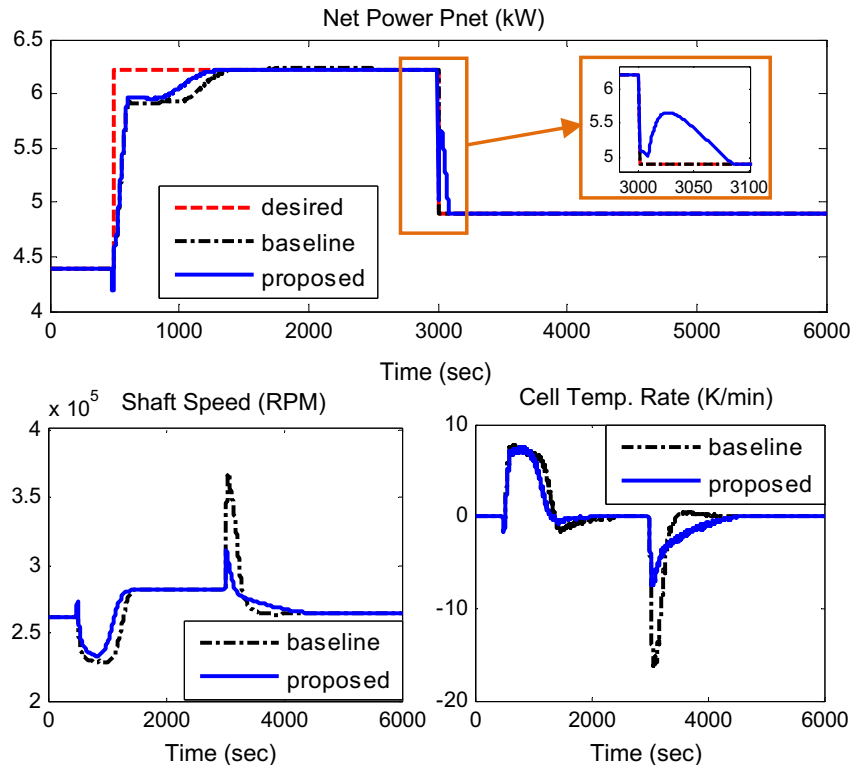


**Fig. 10.** Transient performance of the baseline case and the proposed control strategies during the load transition (step-up from 4.39 kW to 6.23 kW at 500 s and then step-down to 4.90 kW at 3000 s).

charging power  $P_{\max}$  and energy capacity  $E_{\text{brg}}$ , have been achieved through active control of  $P_{\text{gen}}$  in all the other cases.

## 5. Evaluation of the proposed control strategies

The proposed control strategies are evaluated through a typical load transition profile (Fig. 10), in which the pre-conditioning strategy (Section 3.3,  $N_{\text{des}} = 1.02N_{\text{crt}}$ ) is applied during load step-up transition while the coordinated power and thermal control (11) is used for load step-down transition. Compared with the baseline case (LG used for load step-up while the direct  $P_{\text{gen}}$  compensator (10) is used for load step-down), improved load following performance has been achieved during load step-up transition. Meanwhile, the cell temperature change rate is limited in a reasonable range all along the transition, thereby ensuring thermal transient safety.

## 6. Conclusions

To extend the dynamic capabilities of the SOFC/GT-based APU for improved load following performance, the system is augmented by an energy storage device (e.g., battery) and a dual operating generator/motor (G/M). This paper focuses on studying the G/M dual mode operation and its implications on the transient performance and energy storage requirements. Active shaft load control can be achieved by pre-conditioning of the G/M load for load step-up transitions and absorbing the excessive power during load step-down transitions. Feedback and optimization algorithms are proposed to implement the G/M dual mode operation concept. Simulation results demonstrate their effectiveness and computational efficiency. By taking full advantage of the dual operating G/M, better trade-offs between power tracking and thermal safety can be achieved, power and energy requirements for the battery can be reduced, and overall system performance can be enhanced. Future work includes replacing the feedback control with model-based predictive control (MPC) to improve the overall performance for load step-down transitions.

## Acknowledgment

The authors would like to acknowledge Automotive Research Center (US Army TARDEC) and Naval Engineering Education Center (US Navy) for the support of this research.

## References

- [1] S.C. Singhal, K. Kendall, High Temperature Solid Oxide Fuel Cells Fundamentals, Design and Applications, Elsevier, 2003.
- [2] J. Brouwer, Hybrid gas turbine fuel cell systems (chapter 4), in: Richard A. Dennis (Ed.), The Gas Turbine Handbook, U.S. Department of Energy, Morgantown, West Virginia, 2006, DOE/NETL-2006/1230.
- [3] R.A. Roberts, J. Brouwer, E. Liese, R.S. Gemmen, ASME Journal of Engineering for Gas Turbines and Power 128 (2) (April, 2006) 294–301.
- [4] So-Ryeok Oh, Jing Sun, Comparative Performance Assessment of 5kW-class Solid Oxide Fuel Cell Engines Integrated with Single/Dual-Spool Turbochargers. American Control Conference, San Francisco, California, 2011, pp. 5231–5236.
- [5] So-Ryeok Oh, Jing Sun, Herb Dobbs, Joel King, Model-based predictive control strategy for a solid oxide fuel cell system integrated with a turbocharger, to be presented in 2012 American Control Conference.
- [6] Caihao Weng, Jing Sung, Design of a variable geometry turbine control strategy for solid oxide fuel cell and gas turbine hybrid systems, to be presented in 2012 American Control Conference.
- [7] Christoph Stiller, Bjørn Thorud, Olav Bollanda, et al., Journal of Power Sources 158 (1) (July 2006) 303–315.
- [8] Christoph Stiller, Design, operation and control modelling of SOFC/GT hybrid systems, PhD thesis, Department of Energy and Process Engineering, Norwegian University of Science and Technology, Trondheim, Norway, March 2006.
- [9] Vasilis Tsourapas, Control analysis of integrated fuel cell systems with energy recuperation devices, PhD thesis, University of Michigan, Ann Arbor, MI, USA, 2007.
- [10] S. Ibaraki, Y. Yamashita, K. Sumida, et al., Mitsubishi Heavy Industries Technical Review 43 (3) (2006).
- [11] So-Ryeok Oh, Jing Sun, Optimization and Load-Following Characteristics of 5kW-Class Tubular Solid Oxide Fuel Cell/Gas Turbine Hybrid Systems. American Control Conference, Baltimore, MD, USA, 2010, pp. 417–422.
- [12] David Hall, Transient Modeling and Simulation of a Solid Oxide Fuel Cell. PhD thesis, University of Pittsburgh, 1997.
- [13] Thermodynamics Lecture Notes, Section 18.5: Heat Exchangers. <http://web.mit.edu/16.unified/www/FALL/thermodynamics/notes/node131.html>.
- [14] T. Alston, K. Kendall, et al., Journal of Power Sources 71 (1–2) (1998) 271–274.
- [15] V. Lawlor, S. Griesser, G. Buchinger, et al., Journal of Power Sources 193 (2) (2009) 387–399.